ADVANCED ENERGY MATERIALS
www.advenergymat.de

Lithium Intercalation Behavior in Multilayer Silicon Electrodes

Tim T. Fister, Jennifer Esbenshade, Xiao Chen, Brandon R. Long, Bing Shi, Christian M. Schlepütz, Andrew A. Gewirth, Michael J. Bedzyk, and Paul Fenter*

Next generation lithium battery materials will require a fundamental shift from those based on intercalation to elements or compounds that alloy directly with lithium. Intermetallics, for instance, can electrochemically alloy to $Li_{4.4}M$ (M = Si, Ge, Sn, etc.), providing order-of-magnitude increases in energy density. Unlike the stable crystal structure of intercalation materials, intermetallic-based electrodes undergo dramatic volume changes that rapidly degrade the performance of the battery. Here, the energy density of silicon is combined with the structural reversibility of an intercalation material using a silicon/metal-silicide multilayer. In operando X-ray reflectivity confirms the multilayer's structural reversibility during lithium insertion and extraction, despite an overall 3.3-fold vertical expansion. The multilayer electrodes also show enhanced long-term cyclability and rate capabilities relative to a comparable silicon thin film electrode. This intercalation behavior found by dimensionally constraining silicon's lithiation promises applicability to a wide range of conversion reactions.

1. Introduction

Structural and chemical changes associated with the reversible insertion and extraction of lithium in a Li-ion battery electrode are generally categorized as conversion or intercalation reactions.[1] Materials that undergo intercalation, such as graphite or layered lithium metal oxides,[2] maintain the crystalline-like phase of their host structure during Li^+ insertion and extraction; this provides the electrode with structural reversibility, but intrinsically limits the lithium insertion capacity. In contrast, conversion materials alloy with lithium either homogeneously (e.g., Si, Sn)[3] or heterogeneously (e.g., metal oxides, fluorides, sulfides),[4] the latter leading to phase separation into a lithium-rich compound and a reduced parent species.[5] The lithiated phases have distinct, thermodynamically stable, crystallographic phases[6] that are not, however, kinetically accessible near room temperature. As a result, the lithiated products of conversion reactions tend to be amorphous.[7]

Despite their higher energy densities, conversion materials are nearly absent from commercial Li-ion batteries due to their high overpotentials (particularly for heterogeneous materials), diffusion-limited kinetics, and limited reversibility. The latter problem is often associated with the dramatic volume changes caused by their high lithium content. Silicon, for instance, has the highest known gravimetric capacity at 4400 mAh g^{-1}, but expands by nearly 400% at $Li_{4.4}Si$. Repeated cycling pulverizes the electrode, rapidly reducing its overall charge capacity as silicon delaminates from its current collector. Numerous strategies have been introduced to improve the reversibility of conversion materials, particularly silicon.[8,9] Most prominent is the use of nanostructured silicon electrodes, such as nanoparticles or "conditioned" particles,[10] thin films, or nanowires/tubes.[11] These systems are found to reduce overall strain and associated electrode delamination by tailoring the direction of expansion and suppressing crystallization of $Li_{15}Si_4$ found in more bulk-like electrodes.[12] Silicon-based composites with conductive media, such as carbon binders, can also preserve electrical conductivity and cushion any volume changes.[13] Much like particle size in laminates, the cycle lifetime of silicon thin films correlates inversely with their thickness or degree of discharge,[14] which complicates scale-up. Nanostructured silicon electrodes, such as wires[11] or patterned crystals,[15] have shown promising reversibility in half-cells, but often require incomplete lithiation to maintain internal stability during cycling and tend to have low Coulombic efficiency resulting from secondary reactions occurring at the electrode surface.

To date, only a few studies have explored the electrochemical behavior of silicon/metal multilayers,[16,17] notably with

Dr. T. T. Fister, Dr. B. R. Long, Dr. P. Fenter
Chemical Sciences and Engineering Division
Argonne National Laboratory
Argonne, IL, 60439, USA
E-mail: fister@anl.gov
J. Esbenshade, Dr. B. R. Long, Prof. A. A. Gewirth
Department of Chemistry
University of Illinois
Urbana-Champaign, Urbana, IL, 61801,USA
X. Chen
Graduate Program in Applied Physics
Northwestern University
Evanston, IL, USA
Dr. B. Shi, Dr. C. M. Schlepütz
Advanced Photon Source
Argonne National Laboratory
Argonne, IL, 60439, USA
Prof. M. J. Bedzyk
Departments of Materials Science & Engineering and Physics & Astronomy
Northwestern University
Evanston, IL, 60208, USA

DOI: 10.1002/aenm.201301494

Co and Fe. Our recent work on silicon/chromium bilayers revealed preferential lithiation at the intermixed silicide interfaces leading to a stratified heterostructure with an unexpected stability to lithiation/delithiation reactions.[18] This observation suggested that the synergistic use of architectures that combine the energy density of conversion materials with the stability found in layered structures might lead to substantially improved behavior.

Here, we demonstrate that multilayers consisting of alternating amorphous silicon thin films and planar, conducting "adhesive layers" of Cr_xSi ($x \approx 3$) combine the intrinsically high Li-capacity of silicon, the reversibility of ultrathin silicon films, and the conductivity of a composite material. Real-time X-ray reflectivity measurements reveal that the internal layering in the Si/Cr_3Si multilayers is preserved during lithiation and delithiation, strongly enhancing its reversibility. During these reactions, the overall electrode reversibly expands and contracts by a factor of 330% solely in the vertical direction. Extended charging and discharging confirms that the multilayer provides superior reversibility over comparable silicon thin films with potential for high power applications. We discuss the effect of overall thickness and pitch on the reversibility and rate capabilities of silicide multilayers under both voltammetric and galvanostatic cycling conditions. These results suggest that the multilayer architecture is a novel strategy for addressing the extreme challenges associated with silicon and related materials in Li-ion battery electrodes.

2. Results

2.1. Structural Changes Under Potentiostatic Conditions

X-ray reflectivity data from a Si/Cr_3Si multilayer (20 bilayers) under potentiostatic control are shown in **Figure 1**a,b and are stacked sequentially, starting at the top of Figure 1a. The first through n^{th}-order multilayer Bragg peaks (seen clearly at the extreme potentials) appear periodically in momentum transfer q due to the repeated bilayer d-spacing. For the as-grown multilayer, $d_{Si+Cr3Si} = 2\pi/\Delta q = 8.1$ nm based on the higher-order consecutive Bragg peaks that are least affected by refraction. The finer fringes between the Bragg peaks in the as-grown multilayer result from the overall thickness of the film and are directly related to electron density changes at the surface. These surface fringes initially grow in amplitude (at 0.4 V) due to Li^+ surface accumulation that increases the change in surface electron density.[18] As seen in the subsequent reflectivity curves in Figure 1a, the surface fringes rapidly diminish below 0.4 V as the surface roughens in response to lithiation. At the same time, the multilayer Bragg peaks from the starting 8.1-nm periodicity decrease in intensity and new Bragg peaks begin to appear, especially at lower q. As the potential is held at 0.01 V, Bragg peaks corresponding to a bilayer d-spacing of 26.7 nm grow in intensity as the layering becomes more coherent. In all cases, the reflectivity data are modulated by a long period oscillatory background corresponding to the unlithiated Cr_3Si layers which remain 1.9 nm thick.

Upon delithiation (Figure 1b), the Bragg peak amplitude of the lithiated structure rapidly decreases in height and d-spacing, indicating contraction of the lattice with a variable layer thickness. From 2–3 V, the reflectivity continues to exhibit very little structural order except for a broad oscillation (corresponding to the 1.9 nm thickness of the unaffected Cr_3Si layers) and several low-q multilayer peaks, indicating that the silicon layers still lack a consistent d-spacing. After increasing the voltage above the open circuit condition to 3.5 V, sharper Bragg peaks immediately reappear near their original position with a spacing corresponding to a 9.3 nm thick bilayer with a surprisingly coherent layered structure.

The cyclic voltammogram taken simultaneously with the reflectivity data, shown in Figure 1c, has features characteristic of silicon electrochemistry.[19] Figure 1d depicts the overall expansion and contraction of the multilayer by 330% at the extreme potentials. These results reveal a process, under potentiostatic conditions, in which individual layers delithiate at varying potentials, but that the vertical structure becomes laterally homogeneous once it is equilibrated at extreme potentials.

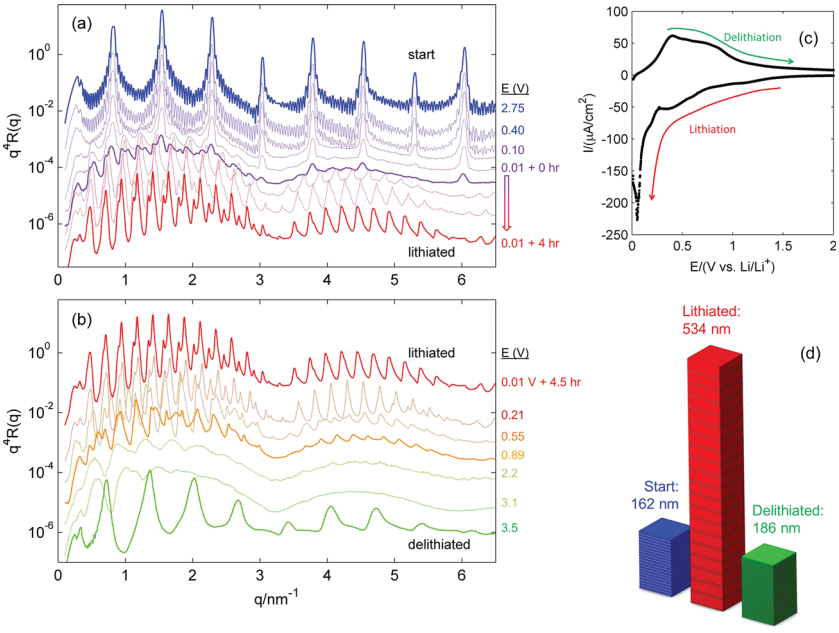

Figure 1. Selected reflectivity curves during a) lithiation and b) delithiation. Reflectivity $R(q)$ has been scaled by q^4 to remove the sloping Fresnel background and offset for clarity. The average potential during each scan is labeled on the right side of the plot. Two intermediate conditions are highlighted in purple and orange during lithiation and delithiation. c) Cyclic voltammogram taken during the measurement at 0.2 mV s^{-1}. The sample was also held at 0.01 V for 4.5 h. d) Schematic highlighting the multilayer's extreme height change during lithiation and delithiation.

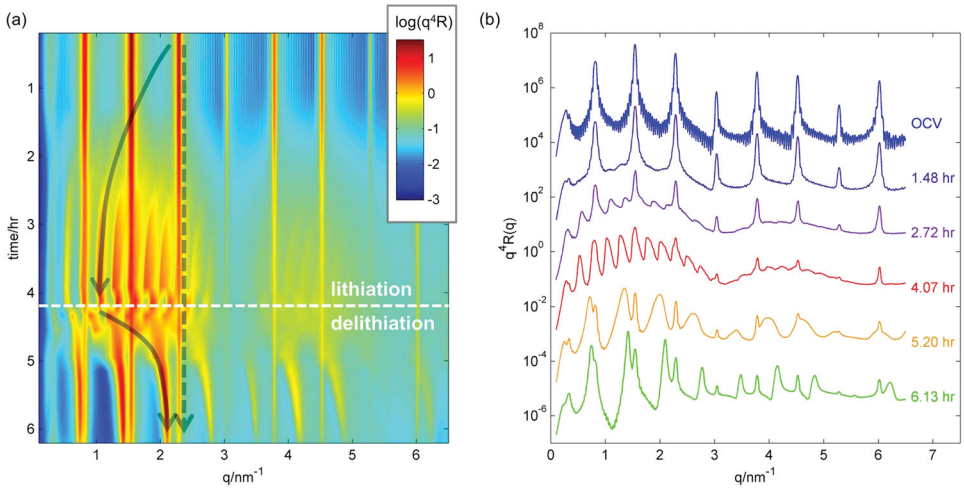

Figure 2. a) Data taken continously during the 60 μA cm^{-2} discharge/charge is shown as a 2D density plot. Solid curves follow the path of the 3rd order Bragg peak during lithiation and delithiation; a dashed, gray line highlights the unlithiated 3rd order peak. b) Selected curves from (a) are shown for comparison to the potententiostatic conditions shown in Figure 1. Curves are offset for clarity. Note the coexistance of unlithated and lithiated phases in each case.

2.2. Structural Changes Under Galvanostatic Conditions

Similar measurements taken at constant current (i.e., galvanostatic conditions) reveal a laterally heterogeneous lithiation process. Reflectivity curves taken in real-time at 60 μA cm^{-2} (corresponding to a two hour charge rate) are shown in **Figure 2**. These reflectivity data show a coexistence of Bragg peaks corresponding to both lithiated and unlithiated phases throughout the cycling. At the onset of lithiation (delithiation), the new set of Bragg peaks shift rapidly in q indicating a fast, coherent expansion (contraction).

3. Discussion

The differences in reflectivity between Figure 1 and Figure 2 suggest two distinct routes for lithiation and delithiation under potentiostatic and galvanostatic conditions. Under controlled potential, the lack of diffraction peaks at intermediate lithiation or delithiation indicates a structure with varied silicon layer thicknesses. Since layer thickness corresponds to the degree of lithiation, the lack of Bragg peaks at intermediate lithation suggest that lithium is transported vertically, i.e., layer-by-layer, through the multilayer. In contrast, the persistent diffraction peaks from partially lithiated and (especially) delithiated phases are clearly visible during intermediate conditions in Figure 2, indicating that these layers expand and contract with nominally uniform lattice spacing under galvanostatic conditions. The origins of this effect can be traced to the aforementioned coexistance of lithiated and unlithiated phases. The boundary between these two phases creates defects, such as cracks, that provide access to the multilayer's edge-plane leading to a uniform degree of lithiation in each layer. This effect is most visible during delithiation, i.e., following defect formation, and can be clearly seen in the 5.2 h. curve shown in Figure 2b. The two scenarios corresponding to potentiostatic and galvanostatic lithiation are illustrated in **Figure 3**.

To quantify changes in the multilayer structure upon lithiation, we analyze the Fourier transform of the Fresnel-normalized reflectivity. Essentially a 1D Patterson function, this quantity is the autocorrelation function for the derivative of the electron density $\rho(z)$ within the kinematic limit for reflectivity. As discussed at length in the Supporting Information,

$$\frac{R(q)}{R_F(q)} = \left| \int e^{-iqz} \frac{\partial \rho}{\partial z} dz \right|^2 \Rightarrow \langle \rho'(z)\rho'(z') \rangle = \left| \int e^{iqz} \frac{R(q)}{R_F(q)} dq \right|^2$$

where R_F is the calculated Fresnel reflectivity for the Si/electrolyte system.

For step-wise density profiles, this quantity directly reveals internal spacings in the multilayer structure. Similar approaches are well-established for reflectivity[20] and X-ray diffraction in general.[21] As depicted in **Figure 4**a, the correlation associated with the thickness of an individual layer in a series of alternating layers is negative since it results from the product of a positive and negative change in density at its boundaries. Similarly, the bilayer thickness is indicated by a positive.

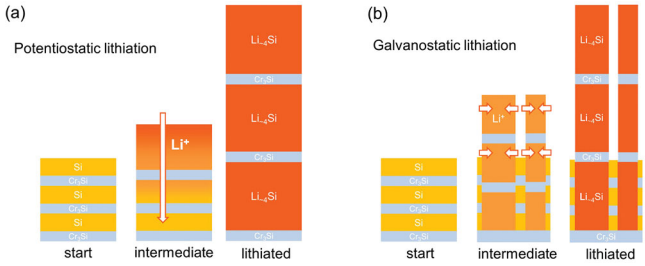

Figure 3. Structural differences between potentiostatic and galvanostatic lithiation are illustrated in panels (a) and (b), respectively. The mechanism is based on the position and distribution of multilayer diffraction peaks during lithiation and delithiation. The color and height of the individual silicon layers in the illustration indicates the degree of lithiation and arrows indicate the inferred direction of lithium transport.

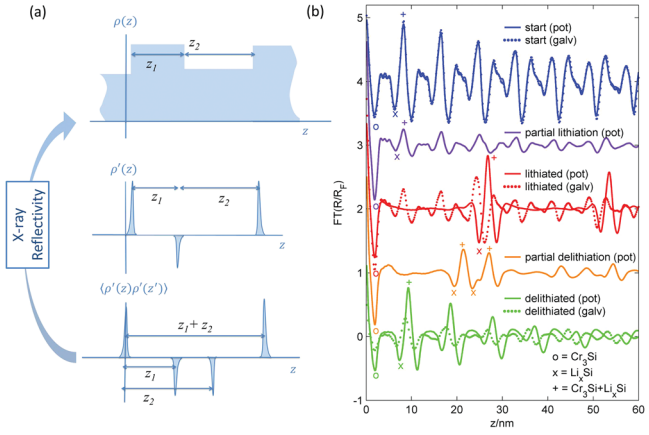

Figure 4. a) Example of Patterson function for a multilayer. From top to bottom: the electron density for the repeated bilayer, its derivative, and the autocorrelation function for the derivative. b) Patterson functions for the initial, lithiated, and delithiated multilayer structures (3, 0.01, and 3.5 V respectively) and intermediate stages. The curves have been offset for clarity and the first three peaks are labeled according to the lower right key. The colors of the curves correspond to the conditions shown in Figure 1,2. The galvanostatic correlation functions overlay the extreme conditions lithiation.

In such a multilayer, these three peaks are repeated in the Patterson function and decay in intensity as a function of the overall coherency of the layer spacing.

Patterson functions for the five highlighted conditions in Figure 1 are shown in Figure 4b. In the starting case (the open-circuit condition), the repeated three peak pattern can be attributed to the Cr_3Si, silicon, and bilayer thicknesses of 1.9, 6.2, and 8.1 nm, respectively. After potentiostatic lithiation, the bilayer consists of Cr_3Si, Li_xSi, and bilayer layers of 1.9, 24.8, and 26.7 nm thicknesses, respectively. The silicon layers' four-fold expansion is consistent with full lithiation to $Li_{4.4}Si$. The galvanostatic case, given by the overlaid dashed curves at the extreme conditions, is more complicated. Lithiation only consumes part of the sample, as Patterson features from the original structure persist. The amplitude of the peaks during lithiation and delithiation is also comparatively muted and decays faster, indicating vertical disorder. As discussed in the supplementary information, the full width at half maximum (FWHM) of the lithiated multilayer's Bragg peaks also increases quadratically in q, indicating weak paracrystalline order.

4. Extended Electrochemical Characterization

The high structural reversibility observed by X-ray reflectivity when these silicon-rich multilayers undergo an overall 3.3-fold vertical expansion and contraction during lithiation suggests that this architecture bypasses the known mechanical instabilities of lithiated silicon anodes. We evaluated the electrochemical stability of these multilayers by lithiation/delithiation cycling in a half-cell battery (i.e., versus a lithium metal counter electrode). For these tests, multilayers were deposited on copper foil and compared to thin Si films with the same overall silicon thickness (**Figure 5**a). Both the 100 nm-thick silicon film and the 5/2 × 20 multilayer (5 nm Si on 2 nm

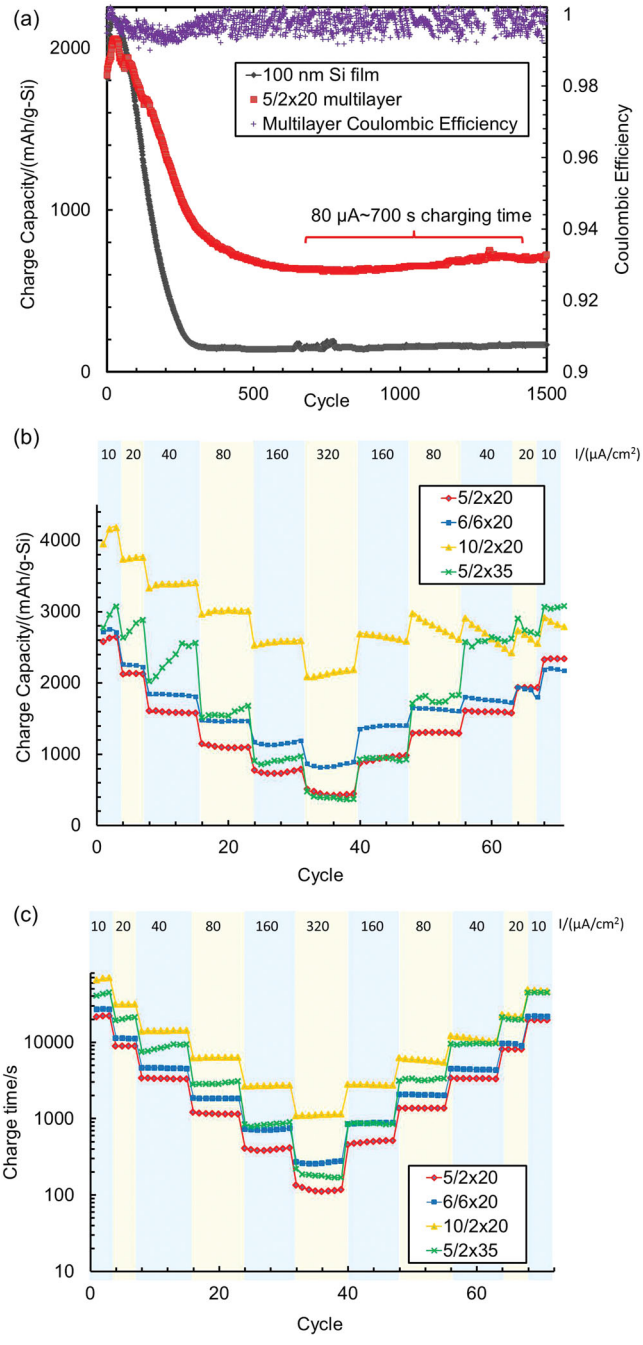

Figure 5. a) Cycling data for a multilayer (5/2 × 20 = 5 nm Si/2 nm Cr_3Si, repeated 20 times) compared to a thin film with same overall silicon thickness (100 nm) grown on copper foil. Each sample was cycled at 80 μA cm^{-2} between 3 and 0.01 V. While both electrodes show a performance loss between cycles 50 and 300, the multilayer significantly outperforms the thin film thereafter. b,c) Rate studies measuring the capacity and charging time for multilayers with varying layer thickness and number of layers. In each case, the naming convention corresponds to (Si thickness in nm)/(Cr_3Si thickness in nm) × (repetitions). All multilayers show diffusion-limiting transport. In general, thicker Cr_3Si and, especially, Si layers show somewhat reduced reversibility.

Cr_3Si repeated 20 times) initially show stable 2000 mAh g^{-1} capacity (cycled at 80 μA cm^{-2}), although with a systematic loss of capacity between cycles 40–300. During this period, the

Coulombic efficiency decreases to ≈99.5%. While the thin film eventually loses nearly all of its lithiation capacity, the multilayer retains ≈750 mAh g^{-1}-Si capacity with consistent charge/discharge density in this region. Furthermore, at this applied current, the electrode has an extremely fast charging time of 700 s. Diffusion limitations appear to be limiting the capacity in this regime. When cycled at 4 μA cm^{-2}, a multilayer with the same *d*-spacing showed nearly the full theoretical capacity (≈4000 mAh g^{-1}-Si; see Supporting Information). One of the most attractive features of the multilayer is that it has an extremely high Coulombic efficiency: 99.78% over the whole cycle range and 99.89% over the last 1000 cycles, which is well beyond efficiencies for most silicon electrodes, particularly high surface-area 3D nanostructures.[11] The efficiency is expected to be higher for thicker multilayers structures that have smaller area-to-volume ratios and for multilayers cycled at less extreme voltages.

We examined the diffusion limitations of the Si/Cr_3Si multilayers by cycling four types of multilayers grown on copper foil at variable rates (doubling the current between 10–320 μA cm^{-2}. The multilayer given in Figure 5a (5/2 × 20) was compared to multilayers containing thicker silicon layers (10 nm, i.e., 10/2 × 20), thicker Cr_3Si layers (6 nm, i.e., 6/6 × 20), and a structure with a larger number of layers (35 layers, i.e., 5/2 × 35). As seen in Figure 5b,c, each multilayer shows a power law behavior associated with diffusion limitations of lithium in the silicon; that is, the capacity decreases linearly as the current is doubled in this regime. With the largest overall amount of silicon, the 10/2 × 20 multilayer initially has the largest overall capacity since its current/mass ratio is the lowest of all the structures; however, this structure also shows irreversible losses as the structure is returned to slower cycling rates, in particular after cycle 40. In contrast, the 5-nm silicon multilayers show greater reversibility, even after charge times of only ≈100 s at 320 μA cm^{-2}. In fact, the 35 layer structure shows a capacity enhancement during the initial cycling and on the return to slower cycling, possible due to the creation of defects over time, as discussed above and in Figure 3b. The average Coulombic efficiency over the 71 cycles shown was >99% in all cases.

5. Conclusions

These studies demonstrate that combining a highly lithium-reactive material, such as silicon, with thin metallic interlayers in a digitized vertical structure is a new route toward achieving the fast kinetics of nanoscale thin films with improved lifetimes and significantly higher capacities (i.e., thicker overall electrodes). In operando X-ray reflectivity reveals that the layered structure remains intact despite a 3.3-fold vertical expansion and contraction during lithiation. Thus, it retains its 1D "metacrystal" structure, much like a layered intercalation material, but with amorphous components. We conclude that this multilayer architecture, which combines the robust framework with a conversion material (each consisting of amorphous materials), is the key feature that constrains the silicon to purely vertical expansion without delamination, thereby improving reversibility. This general architecture greatly expands the range of materials possible for intercalation in Li-ion batteries, including higher power conversion anodes, such as germanium,[22] or the higher voltage redox couples found in metal fluoride and sulfide cathodes.[23]

6. Experimental Section

Multilayers were grown at room temperature using DC magnetron sputtering by alternating between Cr and Si deposition to form 20 periodic bilayers. Cr was chosen for its adhesion properties, electronic conductivity, and because it does not alloy with Li. As described in the supplementary material, X-ray reflectivity was used to characterize the thickness and density of each layer. In all cases, the 2 nm-thick Cr layer was found to have a density much lower than Cr metal due to intermixing with the adjacent silicon layers. Chromium silicides are known to form even at room temperature,[24,25] and the reflectivity indicates an amorphous layer with density near that of Cr_3Si. Like Cr metal, Cr_3Si is a metallic alloy[26] that does not alloy with Li.[27] The multilayers were grown on Cu electrodes for electrochemical characterization in coin cells and on atomically-flat R-plane sapphire substrates for synchrotron X-ray characterization.

The multilayer structure provides a nano-scale periodicity that can be followed directly using X-ray diffraction even though the individual materials are intrinsically amorphous. Specular X-ray reflectivity measurements (i.e., $q = q_z$) were performed at 20 keV (λ = 0.062 nm) at sector 33BM at the Advanced Photon Source.[28] The X-ray beam (with cross-section of 2 × 0.2 mm^2 and divergence of 40 μrad = 0.005 nm^{-1} along the 2θ direction) illuminated a 2 × 3 mm^2 area on the sample. Data were collected at fine intervals (Δq = 0.005 nm^{-1} using an area detector (Pilatus 100k), allowing for a full 3D reciprocal space measurement of the specular truncation rod. Apart from the substrate, no additional Bragg peaks were found from the silicon or Cr_3Si layers confirming that they were effectively amorphous. Samples were probed in a specially designed spectroelectrochemical cell (using a "transmission-geometry") with a lithium counter/reference electrode and controlled using a CHI760d potentiostat. Both X-ray and coin cell measurements were performed using Li half-cells and all potentials are reported versus the Li/Li^+ redox couple. Reflectivity scans typically took 15 min (1600 data points) and were measured repeatedly during i) voltammetric (ΔE = 0.2 mV s^{-1}) and (ii) galvanostatic cycling (I = 60 μA cm^{-2} between 0.01 and 3.5 V. The samples were held for 2–4 h at the extreme potentials to establish a stable structure in both cases.

Supporting Information

Supporting Information is available from the Wiley Online Library or from the author.

Acknowledgements

This research was supported as a part of the Center for Electrical Energy Storage: Tailored Interfaces, an Energy Frontier Research Center funded by the US Department of Energy, Basic Energy Sciences under award number DE-AC02–06CH11. The beamline staff at 33BM, Advanced Photon Source (APS) provided valuable assistance. Research at sector 33 is supported by the U.S. Department of Energy. Insightful feedback from John Vaughey and Michael Thackeray was greatly appreciated.

Received: October 2, 2013
Revised: November 22, 2013
Published online: January 27, 2014

[1] A. S. Arico, P. Bruce, B. Scrosati, J. M. Tarascon, W. Van Schalkwijk, *Nat. Mater.* **2005**, *4*, 366.
[2] M. S. Whittingham, *Chem. Rev.* **2004**, *104*, 4271.
[3] W. J. Zhang, *J. Power Sources* **2011**, *196*, 877.
[4] J. Cabana, L. Monconduit, D. Larcher, M. R. Palacin, *Adv. Mater.* **2010**, *22*, E170.
[5] P. Poizot, S. Laruelle, S. Grugeon, L. Dupont, J. M. Tarascon, *Nature* **2000**, *407*, 496.
[6] V. L. Chevrier, J. W. Zwanziger, J. R. Dahn, *J. Alloy. Compd.* **2010**, *496*, 25.
[7] P. Limthongkul, Y.-I. Jang, N. J. Dudney, Y.-M. Chiang, *Acta Mater.* **2003**, *51*, 1103.
[8] U. Kasavajjula, C. S. Wang, A. J. Appleby, *J. Power Sources* **2007**, *163*, 1003.
[9] X. Su, Q. Wu, J. Li, X. Xiao, A. Lott, W. Lu, B. W. Sheldon, J. Wu, *Adv. Energy Mater.* **2013**, n/a.
[10] M. N. Obrovac, L. J. Krause, *J. Electrochem. Soc.* **2007**, *154*, A103.
[11] C. K. Chan, H. L. Peng, G. Liu, K. McIlwrath, X. F. Zhang, R. A. Huggins, Y. Cui, *Nat. Nanotechnol.* **2008**, *3*, 31.
[12] T. D. Hatchard, J. R. Dahn, *J. Electrochem. Soc.* **2004**, *151*, A838.
[13] X. Zhao, C. M. Hayner, M. C. Kung, H. H. Kung, *Adv. Energy Mater.* **2011**, *1*, 1079.
[14] H. J. Jung, M. Park, Y. G. Yoon, G. B. Kim, S. K. Joo, *J. Power Sources* **2003**, *115*, 346.
[15] J. L. Goldman, B. R. Long, A. A. Gewirth, R. G. Nuzzo, *Adv. Funct. Mater.* **2011**, *21*, 2412.
[16] Y.-L. Kim, H.-Y. Lee, S.-W. Jang, S.-H. Lim, S.-J. Lee, H.-K. Baik, Y.-S. Yoon, S.-M. Lee, *Electrochim. Acta* **2003**, *48*, 2593.
[17] J.-B. Kim, S.-H. Lim, S.-M. Lee, *J. Electrochem. Soc.* **2006**, *153*, A455.
[18] T. T. Fister, B. R. Long, A. A. Gewirth, B. Shi, L. Assoufid, S. S. Lee, P. Fenter, *J. Phys. Chem. C* **2012**, *116*, 22341.
[19] B. R. Long, M. K. Y. Chan, J. P. Greeley, A. A. Gewirth, *J. Phys. Chem. C* **2011**, *115*, 18916.
[20] B. Bataillou, H. Moriceau, F. Rieutord, *J. Appl. Crystallogr.* **2003**, *36*, 1352.
[21] M. C. Burla, R. Caliandro, B. Carrozzini, G. L. Cascarano, L. De Caro, C. Giacovazzo, G. Polidori, D. Siliqi, *J. Appl. Crystallogr.* **2007**, *40*, 834.
[22] J. Graetz, C. C. Ahn, R. Yazami, B. Fultz, *J. Electrochem. Soc.* **2004**, *151*, A698.
[23] X. L. Ji, K. T. Lee, L. F. Nazar, *Nat. Mater.* **2009**, *8*, 500.
[24] L. Lozzi, M. Passacantando, P. Picozzi, S. Santucci, M. De Crescenzi, *Surf. Sci.* **1991**, *251–252*, 579.
[25] L. J. Chen, *JOM* **2005**, *57*, 24.
[26] E. Mazzega, M. Michelini, F. Nava, *J. Phys. F* **1987**, *17*, 1135.
[27] W. J. Weydanz, M. Wohlfahrt-Mehrens, R. A. Huggins, *J. Power Sources* **1999**, *81*, 237.
[28] E. Karapetrova, G. Ice, J. Tischler, H. W. Hong, P. Zschack, *Nucl. Instrum. Methods. Phys. Res. Sect. A* **2011**, *649*, 52.